International Journal of Pharmaceutics 623 (2022) 121921

Contents lists available at ScienceDirect

International Journal of Pharmaceutics

journal homepage: www.elsevier.com/locate/ijpharm

Ondansetron/Cyclodextrin inclusion complex nanofibrous webs for potential orally fast-disintegrating antiemetic drug delivery

Emmy Hsiung [a,1], Asli Celebioglu [a,*,1], Mehmet Emin Kilic [b], Engin Durgun [c], Tamer Uyar [a,*]

[a] Fiber Science Program, Department of Human Centered Design, College of Human Ecology, Cornell University, Ithaca, NY 14853, USA
[b] Computational Science Research Center, Korea Institute of Science and Technology, Seoul 02792, Republic of Korea
[c] UNAM-National Nanotechnology Research Center and Institute of Materials Science and Nanotechnology, Bilkent University, Ankara 06800, Turkey

ARTICLE INFO

Keywords:
Electrospinning
Cyclodextrin
Ondansetron
Fast disintegrating
Oral drug delivery
Antiemetic treatment

ABSTRACT

Ondansetron (ODS) is an effective antiemetic drug which suffers from limited solubility and bioavailability during oral administration due to first-pass metabolism. However, these limitations can be mitigated through inclusion complexation with cyclodextrins (CDs). In this study, we have reported the electrospinning of polymer-free, free-standing ODS/CD nanofibrous webs (NW), a promising approach for developing a fast-disintegrating delivery system of an antiemetic drug molecule. Highly water soluble hydroxypropyl-beta-cyclodextrins (HPβCD) were used as both complexation agent and electrospinning matrix. The computational study revealed that the 1/2 (drug/CD) stoichiometry was more favorable compared to 1/1. The ODS/HPβCD NW was obtained with higher loading efficiency (~96 %) compared to the control sample of ODS/polyvinyl alcohol (PVA) NW (~80 %). The amorphous distribution of ODS raised by complexation and the highly water-soluble nature of HPβCD resulted into faster and better release profile and quite faster disintegration property (~2 s) in artificial saliva than polymeric ODS/PVA NW. Here, ODS/HPβCD NW was generated in the absence of a toxic solvent or chemical to enable the drug loading in an amorphous state. From all reasons above, ODS/HPβCD NW might be a promising alternative to the polymeric based systems for the purpose of fast-disintegrating oral drug delivery.

1. Introduction

Tablet oral dosage forms of drug delivery are common in use due to their ease of administration, controlled dosages, pain avoidance, and economic benefits (Adepu and Ramakrishna, 2021). For patients who have difficulty swallowing pills, such as pediatric, geriatric, or dysphagic patients, tablets may not be a viable option of drug delivery. An alternative closely followed in the pharmaceutical industry is oral fast disintegrating delivery systems (FDDS) incorporated with active pharmaceutical ingredients (APIs) in the form of solid dosage films, patches, or tablets (Preis, 2015; Singh et al., 2021). These FDDS have a quick dissolution and release of the API in the oral cavity without the need for water. Moreover, they rapidly disintegrate in the oral mucosa and leading to a lessened risk of choking (Baghel et al., 2013). The FDDS are especially favorable for drugs with limited water solubility and low bioavailability, as it avoids first-pass metabolism and thus leads to higher absorption of the API in the body (Singh et al., 2021).

Electrospun nanofibrous webs with APIs has gained recent attention for being a favorable method of forming FDDS due to the various properties of nanofibers including high surface area, high porosity, and mechanical integrity. These favorable properties accelerate the solubility of the APIs in aqueous solutions and improve their efficacy (Manuel et al., 2016). It has been reported in the recent studies that electrospun polymeric nanofibrous webs can be successfully incorporated with APIs such as anti-inflammatory drugs (Yu et al., 2010a, 2009), dietary supplements (Yu et al., 2010b), analgesics (Illangakoon et al., 2014), antihistamines (Akhgari et al., 2016; Abbas et al., 2016), and chemotherapeutics (Wang et al., 2021) as oral FDDS. The amorphous distribution of APIs from electrospun nanofibers is a particularly attractive means of creating FDDS. It has been shown that the electrospinning of polymeric systems results in an amorphous distribution of drug molecules from the evaporation rate of the solvent during electrospinning process (Seif et al., 2015). However, the use of polymeric systems can require toxic solvents to dissolve both polymer and drug

* Corresponding authors.
E-mail addresses: ac2873@cornell.edu (A. Celebioglu), tu46@cornell.edu (T. Uyar).
[1] Contributed equally.

https://doi.org/10.1016/j.ijpharm.2022.121921
Received 13 April 2022; Received in revised form 6 June 2022; Accepted 12 June 2022
Available online 15 June 2022

molecules in the electrospinning solutions. (Seif et al., 2015; Sung and Kim, 2020). The polymer-free nanofibrous webs of cyclodextrin inclusion complexes, which are generated using an aqueous medium without a need for additional toxic solvent or chemicals, might be a favorable alternative to develop FDDS.

Cyclodextrins (CDs) are cyclic oligosaccharides which can form inclusion complexes with various type of compounds with non-covalent interactions (Crini, 2014). It has been shown that complexation with CD increases the water solubility and physicochemical properties of the encapsulated compound and these make CD a favorable choice for poorly water-soluble drug molecules (Saokham et al., 2018). Ondansetron hydrochloride (ODS) is an antiemetic drug often prescribed to combat nausea and vomiting after surgery, chemotherapy, or radiation treatment (Kamranpour et al., 2021). The ODS suffers from the limited aqueous solubility and its bioavailability is at around ~ 60% for tablet administration and it could be increased to ~ 95% with the orally fast disintegrating films (Kanouni et al., 2019; Zhu et al., 2015). In one of the related studies of Cho et al., sulfobutyl-ether derivative of β-CD has been used to enhance the solubility and so the permeability of ODS (Cho et al., 2008). Incorporation of ODS into nanofibers has been achieved previously using polyvinyl alcohol (PVA) to create webs for FDDS (Vuddanda et al., 2016). To the best of our knowledge, polymer-free nanofibrous webs of ODS and CDs which may be an improved means of antiemetic delivery have not been reported in the literature yet.

In this study, the highly water-soluble CD derivative hydroxypropyl-beta-cyclodextrin (HPβCD) was chosen for the inclusion complex formation and electrospinning of ODS. HPβCD has been studied extensively in animal and human trials and has been found to be well tolerated, particularly if it is taken orally (Gould and Scott, 2005). As has been shown previously with different drug molecules, including antibiotics (Celebioglu and Uyar, 2019a), antivirals (Celebioglu and Uyar, 2021), anti-inflammatories (Celebioglu and Uyar, 2019b), and steroids (Celebioglu et al., 2021; Celebioglu and Uyar, 2020), the complexation capabilities of HPβCD make it a suitable means of polymer-free FDDS formation having enhanced drug solubility. The purpose of this study is generating polymer-free electrospun nanofibrous webs of ODS/HPβCD inclusion complexes (IC) for the development of FDDS which may be an alternative to conventional tablet and film forms for drug dosage for antiemetics (Fig. 1). The ODS/PVA nanofibrous web was also generated as control sample. The structural analysis and disintegration/release tests of nanofibrous webs have been carried out by further techniques.

2. Materials and methods

2.1. Materials

Hydroxypropyl-beta-cyclodextrin (HPβCD) (Cavasol W7, DS: ~0.9) was provided by Wacker Chemie AG (USA). The ondansetron hydrochloride (ODS) (>98.0 %, TCI America), polyvinyl alcohol (PVA) (Mw 85,000–124,000, 87–89% hydrolyzed, Sigma-Aldrich), dimethyl sulfoxide (DMSO, >99.9%, Sigma), buffer chemicals (phosphate buffered saline tablet (Sigma Aldrich), sodium phosphate dibasic heptahydrate (Na_2HPO_4, 98.0–102.0%, Fisher Chemical), potassium phosphate monobasic (KH_2PO_4, ≥99.0%, Fisher Chemical), sodium chloride (NaCl, >99%, Sigma Aldrich), and o-phosphoric acid (85% HPLC grade, Fisher Chemical), deuterated dimethyl sulfoxide (DMSO-d_6, 99.8%, Cambridge Isotope) were provided commercially. The required water was distilled by Millipore Milli-Q ultrapure water system (Millipore, USA).

2.2. Electrospinning of nanofibrous web

The inclusion complexes of ODS with HPβCD were prepared in a ~ 1:2 (drug:CD) ratio. First, the HPβCD (180%, w/v) was dissolved in water, and the drug (8 %, w/w) was added to the solution and was stirred overnight at room temperature. For the control samples, HPβCD (180%, w/v), PVA (15%, w/v), and ODS/PVA (8 %, w/w of ODS, 15%, w/v of PVA) solutions were prepared as well. The ODS/PVA solution was prepared such that the percentage of ODS was the same as in the ODS/HPβCD one. The solutions' conductivity and viscosity were measured before electrospinning. To measure the conductivity, a conductivity-meter was used (FiveEasy, Mettler Toledo, USA) at room temperature; viscosity was measured using a rheometer (AR 2000 rheometer, TA Instrument, USA) with a 20 mm, 4° cone-plate spindle, at a shear rate of 0.01 to 1000 s^{-1} at 20 °C. The viscosity values which

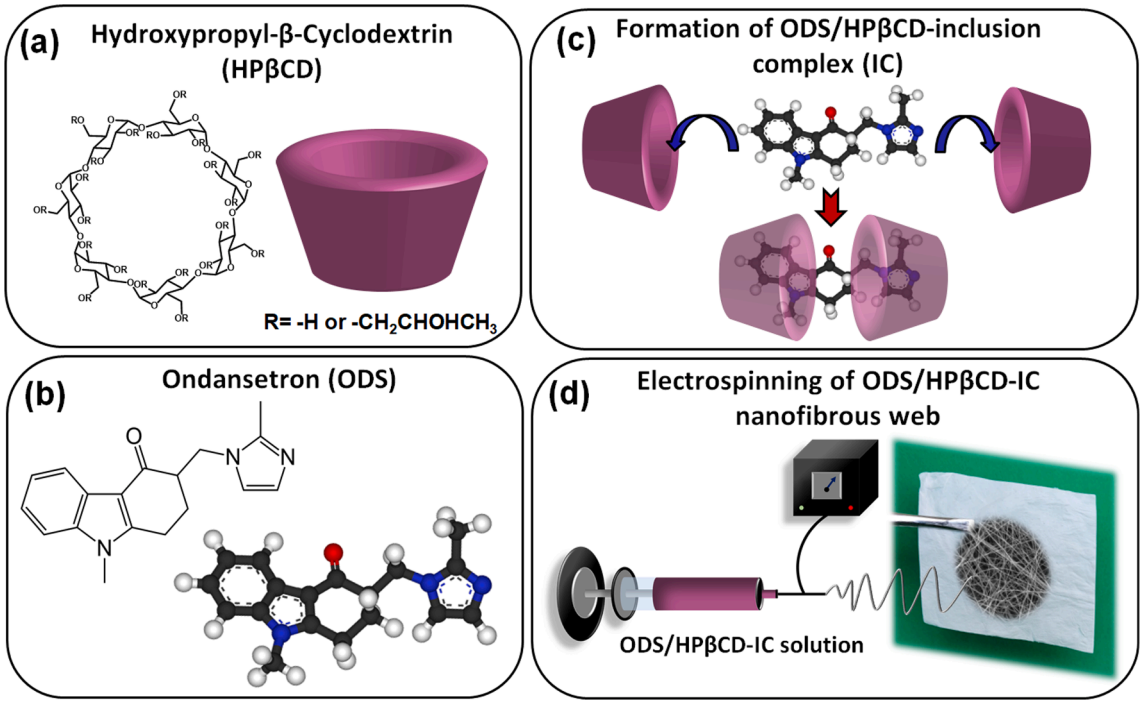

Fig. 1. The chemical structure of (a) HPβCD and (b) ODS. (c) The schematic representation of inclusion complex formation between HPβCD and ODS, (c) and the electrospinning of ODS/HPβCD-IC nanofibrous web.

indicated consistency in the range of 200–800 s^{-1} shear rate were considered to determine the viscosity of the electrospinning solutions. For electrospinning, each solution was individually loaded into disposable plastic syringes with a 23 G needle and placed into electrospinning equipment (Spingenix, model: SG100, Palo Alto, USA) having horizontal configuration. A high voltage of 15 kV was supplied to the stainless-steel needle while the electrospinning solution was being pushed through the syringe at a steady rate of 0.5 mL/h. The nanofibers were deposited on a collector plate covered in aluminum foil 15 cm away from the syringe. The temperature and relative humidity were recorded as ~ 20 °C and ~ 60%, respectively. Besides nanofibrous webs, the physical mixture of ODS/HPβCD powder having the same molar ratio of ~ 1:2 (drug:CD) was also formed as a control by the blending ODS and HPβCD till having a homogenous mixture.

2.3. Physicochemical characterization

The scanning electron microscope (SEM, Tescan MIRA3, Czech Republic) images of nanofibrous webs were obtained to analyze fiber morphology. All samples were sputtered with the thin layer of Au/Pd prior the measurement. The average diameter (AD) of nanofibers (n = ~100) was verified by ImageJ software and given as average diameter ± standard deviation. Attenuated total reflectance Fourier transform infrared (ATR-FTIR) spectrometer (PerkinElmer, USA) was used to record the FTIR spectra of ODS powder, ODS/HPβCD physical mixture, and all nanofibrous webs. The absorption was recorded from 4000 − 600 cm^{-1} at a resolution of 4 cm^{-1} for 32 scans. X-ray diffractometry (XRD, Bruker D8 Advance ECO) was used to determine the X-ray diffraction patterns of ODS powder, ODS/HPβCD physical mixture, and all nanofibrous webs in the range of 2Θ = 5°-30° (Cu-Kα radiation, 40 kV and 25 mA). Thermal profiles of samples were obtained using differential scanning calorimetry (DSC, Q2000, TA Instruments, USA) and thermogravimetric analyzer (TGA, Q500, TA Instruments, USA). For DSC, the samples were loaded into a Tzero aluminum pan and heated at a rate of 10 °C/min from 0 °C to 250° (N_2). For TGA, the samples were heated in a platinum pan at a rate of 20 °C/min from 30 °C to 600 °C (N_2).

2.4. Loading efficiency test

To calculate the loading efficiency of samples, a fixed amount of ODS/HPβCD and ODS/PVA nanofibrous webs (2 mg) were dissolved in DMSO (5 mL). The ODS content was measured using UV − vis spectroscopy, (Perkin Elmer, Lambda 35, USA) (300 nm), and a calibration curve of ODS in DMSO was taken with linearity and acceptability of $R^2 \geq 0.99$. The loading efficiency percentage was calculated using the following equation.

$$\text{Loading efficiency } (\%) = Ce/Ct \times 100 \quad (1)$$

where Ce is the concentration of loaded ODS and Ct the initial concentration of ODS in the nanofibrous samples. The results were repeated at least three times to obtain an average ± standard deviation. Proton nuclear magnetic resonance (^{1}H NMR, Bruker AV500 equipped with autosampler) measurements were also utilized to examine the chemical structure of drug for the ultimate samples and to calculate the loading efficiency of ODS in nanofibrous webs roughly. ^{1}H NMR solutions of samples were prepared in *d6*-DMSO at the sample concentration of 40 mg/mL and spectra were recorded by 16 scans. Mestranova software was used to process the data.

2.5. Computational methodology

The first-principles density functional calculations (Hohenberg and Kohn, 1964; Kohn and Sham, 1965) were performed with the Vienna Ab initio Simulation Package (VASP) (Kresse and Furthmüller, 1996) to reveal the inclusion complex formation between ODS molecules and HPβCD. The Perdew-Burke-Ernzerhof (PBE) form of generalized gradient approximation (GGA) was used to estimate the exchange and correlation energy terms (Perdew et al., 1997). The electron–ion interactions were described with the projector-augmented-wave approach (Blöchl, 1994). The van der Waals interactions were included to GGA-PBE functional by considering empirical dispersion correction (DFT-D2) (Grimme, 2006). The kinetic energy cut-off which determines the plane-wave basis set size, was set to 520 eV. The conjugate gradient method was used to relax the ions by setting the total energy and force (on each atom) convergence criteria to 10^{-5} eV and 10^{-2} eV/A, respectively. The solvent effect was computed by implementing an implicit solvation approach (VASPsol) based on a self-consistent continuum model (Mathew et al., 2016, 2014).

2.6. Pharmacotechnical properties

For phase solubility test, excess amount of ODS was mixed with increasing concentrations of HPβCD, ranging from 0 to 160 mM, in 5 mL of water. It was shaken on an orbital shaker at 450 rpm at room temperature shielded away from light. After 24 h, the solutions were filtered using a 0.45 μm PTFE filter, and the UV–vis spectroscopy was used to measure the absorbance intensity at 210 nm. The measurements were repeated three times for each HPβCD concentrations to obtain an average ± standard deviation. To plot the phase solubility diagram, the calibration curve ($R^2 \geq 0.99$) of ODS in water was used for converting absorbance intensity into concentration (mM). Additionally, the binding constant (K_S) was determined from the linear part of the phase solubility diagram by using the following equation.

$$K_S = \text{slope}/S_0(1\text{-slope}) \quad (2)$$

where S_0 is the intrinsic solubility of ODS (~5.6 mM).

To determine the time-dependent release profiles, the same amount of ODS/HPβCD and ODS/PVA nanofibrous webs (~5 mg) were immersed in 5 mL of PBS buffer solution (pH 7.4). The samples were placed on an orbital shaker at 200 rpm at 37 °C. Aliquots of 200 μL were removed from each sample and replaced with 200 μL of fresh PBS buffer at set time intervals. The UV spectra were recorded at 210 nm (n = 3). The dissolution of the nanofibrous webs was recorded using approximately 5 mg of nanofiber in 5 mL of distilled water (Video-S1). On the other hand, the disintegration profiles of ODS/HPβCD, HPβCD, PVA, and ODS/PVA nanofibrous webs were observed in an artificial saliva environment (pH 6.8; 2.38 g Na_2HPO_4, 0.190 g KH_2PO_4, 8 g NaCl and few drops of phosphoric acid in 1L water) to simulate disintegration in the oral cavity. Filter paper (Fisherbrand, P5 Grade, ϕ: 7 cm, medium porosity, cellulose) was placed in petri dishes (ϕ: 10 cm) and wetted with 10 mL of the artificial saliva solution. The excess medium was drained after keeping systems like that for 10 s and then nanofibrous webs having dimensions of ~ 2.5 X 3.0 cm were placed individually on the wetted filter papers. Simultaneously, a video was filmed of the disintegration of samples (Video-S2 and S3).".

2.7. Statistical analysis

The results of the replicated experiments were given as mean values ± standard deviations. The one-way or two-way of variance (ANOVA) were applied for the statistical analyses. The OriginLab (Origin 2021, USA) was used for the ANOVA analyses (0.05 level of probability).

3. Results and discussion

3.1. Morphology of nanofibrous webs

In this study, ~ 1:2 (drug:CD) molar ratio was applied to prepare the electrospinning solution of ODS/HPβCD system which corresponds to 8

% (w/w) of ODS content in the ultimate nanofibrous webs (NW). The control sample of ODS/PVA NW was prepared with the same ODS content of 8 % (w/w). The pristine HPβCD NW and PVA NW were also generated as control samples. Fig. 2 indicates the optical photos and SEM images of HPβCD NW, ODS/HPβCD NW, PVA NW and ODS/PVA NW. All samples were formed with reasonable flexibility, foldability (Fig. 2-i) and homogenous morphology (Fig. 2-ii). The solution properties (viscosity and conductivity) and the average diameter (AD) of samples were summarized in Table 1. As expected, the addition of ODS increased the viscosity of solution. The conductivity of the HPβCD solution also amplified due to the existence of HCl salt in the formulation of ODS which increased number of ions in the solution (Table 1). Even the viscosity of the solution increased, the electrospinning jet of ODS/HPβCD was exposed to higher stretching effect depending on its distinctively higher conductivity values compared to pure HPβCD solution, so thinner fibers was formed in case of ODS/HPβCD system (115 ± 45 nm) compared to HPβCD one (260 ± 60 nm) (Xue et al., 2019). The polymer-based systems of PVA depicted a similar trend in terms of conductivity and viscosity values (Table 1). However, thicker nanofibers having a ribbon shape were generated for ODS/PVA system (775 ± 315 nm) when compared to PVA (330 ± 55 nm) one. The ribbon-shaped flat fibers were formed by the collapsing of polymer skin layer on the solvent rich interior part of electrospinning jet. It has been reported that the high viscosity and the conductivity of the electrospinning solutions might be the reasons for the formation of ribbon like morphology (Itoh et al., 2016). The high viscosity of solution might hinder the solvent molecules at the core of electrospinning jet and so they could not dissipate which resulting in the polymer skin. In case of high conductivity, the ionic mobility might promote the jet velocity and this might boost the rapid drying of jet which can again cause the polymer skin formation (Itoh et al., 2016).

3.2. Physicochemical properties

Fourier transform infrared (FTIR) spectroscopy was used for the structural analyses of samples (Fig. 3). In case of HPβCD, peaks at 3324–3355 cm^{-1}, 2930 cm^{-1}, 1650 cm^{-1} and 1370 cm^{-1} correspond to –OH stretching, C-H stretching, O-H bending and $–CH_3$ bending of CD, respectively. The absorption bands at 1028 cm^{-1}, 1150 cm^{-1}, and 1180 cm^{-1} correspond to coupled C-C/C-O stretching and antisymmetric C-O-C glycosidic bridge stretching of CD (Yuan et al., 2015). For the FTIR spectrum of ODS, distinct absorption bands were found at 3500–3220 cm^{-1}, corresponding with N-H stretching, 1634 cm^{-1}, corresponding with C = O stretching, 1580 cm^{-1}, 1530 cm^{-1}, 1478 cm^{-1}, 782 cm^{-1}, and 750 cm^{-1}, corresponding with phenyl C-H bending (Teaima et al., 2020; Vuddanda et al., 2016). It is notable that various ODS peaks were inhibited in the FTIR spectrum of ODS/HPβCD NW (Fig. 3a). On the other hand, ODS peaks at 1634 cm^{-1} and 1530 cm^{-1} shifted respectively to 1638 cm^{-1} and 1538 cm^{-1} with a broadening profile supporting the inclusion complex formation (Mura, 2015). In case of ODS/HPβCD physical mixture (PM), there are peaks at 1634 cm^{-1}, 1530 cm^{-1}, and 782 cm^{-1} that aligned directly with the FTIR of pure ODS indicating the lack of specific interaction between the ODS and HPβCD, as would be expected of the physical mixture. In FTIR spectrum of ODS/PVA NW, peaks corresponding to ODS were observed at 1627 cm^{-1}, 1581 cm^{-1}, 1531 cm^{-1}, 1482 cm^{-1}, and 753 cm^{-1} with slight shifts compared to pure ODS peaks (Fig. 3b). As reported in a related study of Vuddanda et al., these shifts can be attributed a possible intermolecular hydrogen bonding between ODS and PVA (Vuddanda et al., 2016).

X-ray diffractometry (XRD) was used to examine the crystalline patterns of samples. Fig. 4a shows the XRD graphs of the ODS powder, ODS/HPβCD PM and nanofibrous webs. ODS has a crystalline structure with distinct peaks at $2\theta \approx 6$, 12.5, 16.5, 20, 23, 24, 25.5, and 28. The characteristic peaks of ODS were detected clearly for ODS/HPβCD PM at $2\theta \approx 6$, 12.5, 16.5, 23, and 25.5. In contrast, any peaks corresponding ODS was not observed at the XRD graph of ODS/HPβCD NW indicating that inclusion complexation with HPβCD broke apart the ODS crystalline structure and allowed it to take on an amorphous distribution within the nanofibrous webs. In the case of ODS/PVA NW, a few ODS peaks were noticed at low intensities with slight shifts corresponding with the FTIR results where potential interaction between PVA and ODS was confirmed evidently (Vuddanda et al., 2016). The differential scanning calorimetry (DSC) finding suggested also the amorphization of ODS within the ODS/HPβCD NW (Fig. 4b). ODS powder indicated a distinct endothermic peak at ~ 185 °C representing the melting point of this crystal drug molecule and additional peak at ~ 90 °C attributed to dehydration of water (Fig. 4b). The endothermic peak taking part in the range of 40–120 °C for HPβCD based samples was also due to the dehydration of water. The melting peak of ODS was notably absent from the DSC graph of ODS/HPβCD NW (Fig. 4b). This lack of an endothermic melting point indicated that ODS was incorporated into sample amorphously, and no longer had a crystalline structure owing to complexation with HPβCD, aligning with the XRD results (Fig. 4a). On the other hand, the melting point of ODS at 185 °C was present in the DSC graph of

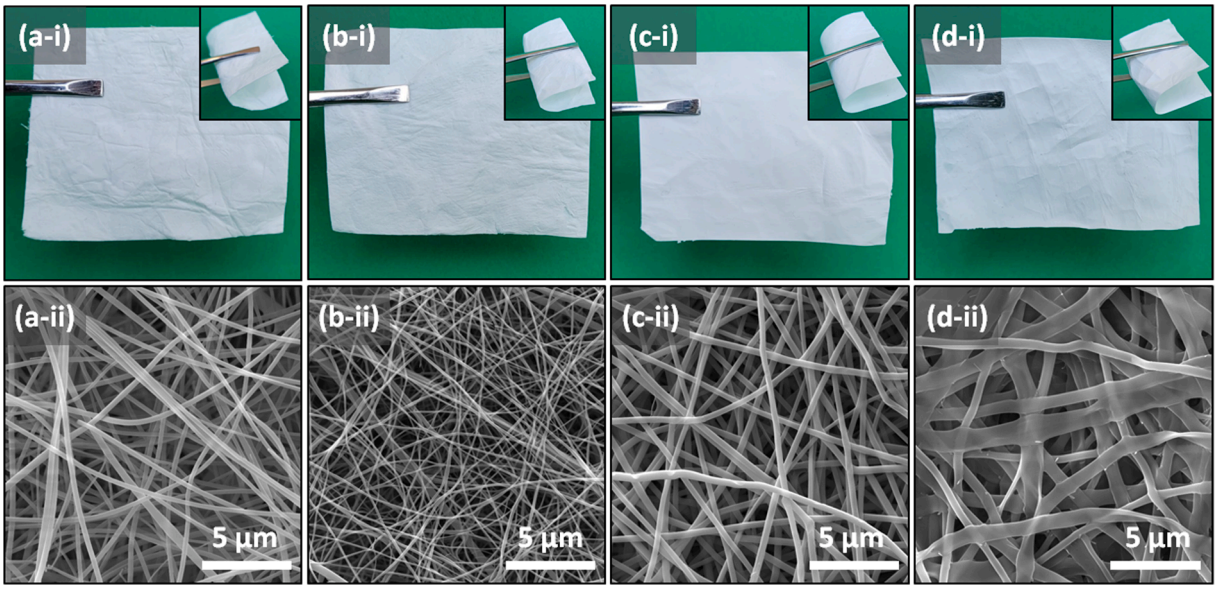

Fig. 2. (i) Photos and (ii) SEM images of (a) HPβCD NW, (b) ODS/HPβCD NW (c) PVA NW, and (d) ODS/PVA NW (NW: nanofibrous web).

Table 1
The solution properties and fiber diameters of resulting nanofibrous webs.

Sample	PVA conc. (%, w/v)[a]	HPβCD conc. (%, w/v)[a]	ODS conc. (%, w/w)[b]	Viscosity (Pa·s)	Conductivity (μS/cm)	Average diameter (nm)
HPβCD	–	180	–	0.4407	45.1	260 ± 60
ODS/HPβCD	–	180	8	0.6994	504.6	115 ± 45
PVA	15	–	–	0.9895	818.8	330 ± 55
ODS/PVA	15	–	8	1.6510	2743.0	775 ± 315

[a] with respect to solvent (water); [b] with respect to total sample amount.

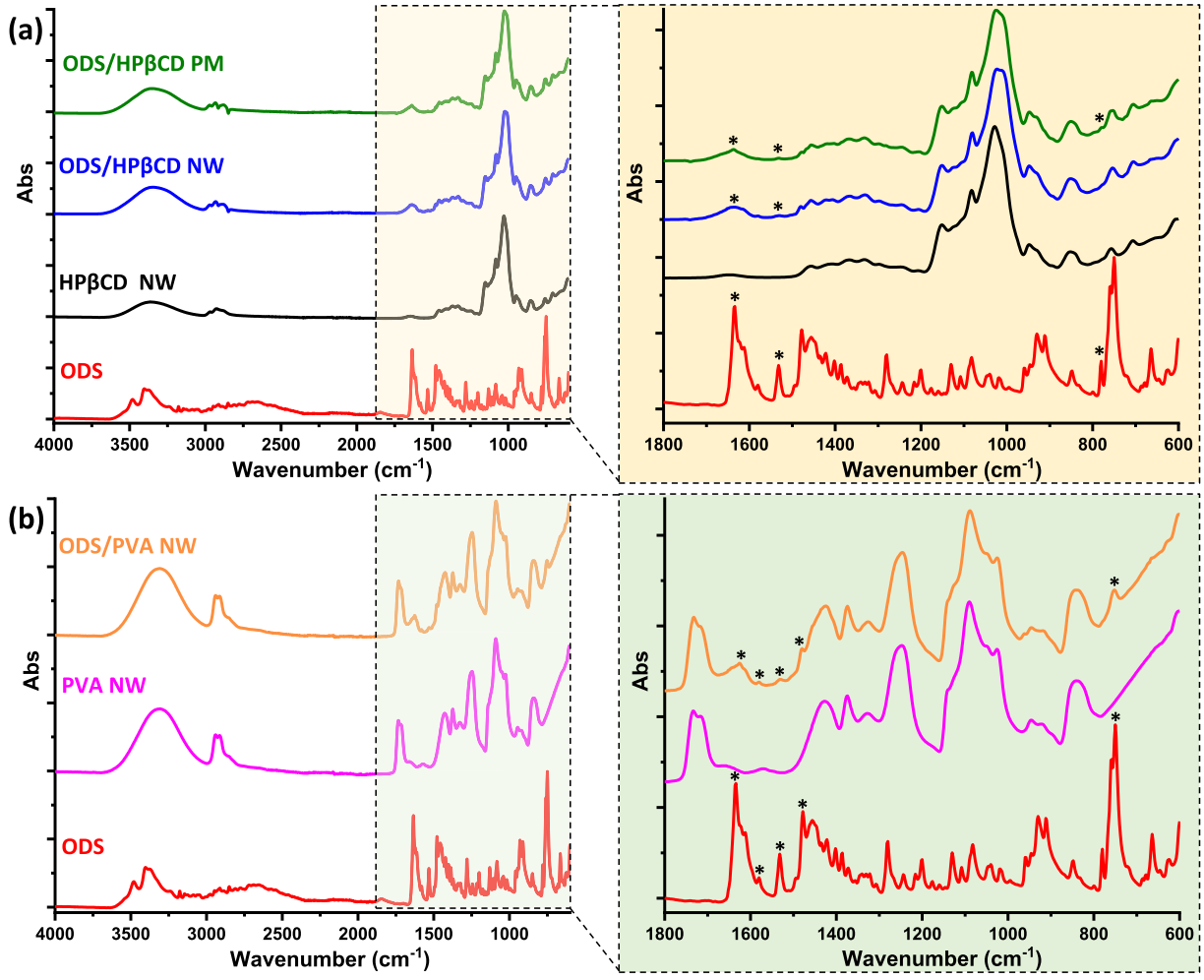

Fig. 3. The full and expanded range FTIR spectra of (a) ODS powder, HPβCD NW, ODS/HPβCD NW, ODS/HPβCD PM, and (b) ODS, PVA NW, and ODS/PVA NW (NW: nanofibrous web; PM: physical mixture).

ODS/HPβCD PM indicating the crystalline state of the drug in the physical mixture. As is observed in Fig. 4c, PVA NW had a broad peak at the range of 30–110 °C corresponding to dehydration and an additional one at 192 °C due to melting of polymer. For ODS/PVA NW, the overlapping melting peaks of ODS (185 °C) and PVA (192 °C) made it hard to identify them separately. However, there was detected a shift of melting point to a lower temperature (187 °C) with the addition of ODS in the PVA system compared to pure PVA (192 °C) suggesting the potential interaction between the PVA matrix and ODS that was also confirmed by the analysis of FTIR (Fig. 3).

The thermal degradation profiles of samples were examined using thermal gravimetric analysis (TGA) (Fig. 5). TGA thermograms of HPβCD NW showed two weight losses; first one at 100°C was due to evaporation of water from the sample, and the next one at 356 °C corresponded to the main degradation of HPβCD. The thermogram of ODS powder showed three weight losses; the first one at 100 °C was again due to evaporation of water, the second and third at 248 °C and 390 °C, respectively corresponded to the thermal degradation of ODS (Tanveer et al., 2021). In case of ODS/HPβCD NW, three steps of weight losses were detected in line with the combination of ODS and HPβCD (Fig. 5a-i). Except for the first weight loss at 100 °C, there was noticed a significant difference in the derivative thermogram (DTG) profile of ODS/HPβCD NW compared to individual thermograms of ODS and HPβCD (Fig. 5a-ii). First, the main degradation step having peak value at 280 °C showed an onset point at 230 °C which was substantially higher than the main degradation step of pure ODS (160 °C). Secondly, even HPβCD constituted a huge part of the ODS/HPβCD NW with ~ 90 % (w/w), the next peak observed at 350 °C and matched with the main degradation of HPβCD (356 °C) within the nanofibrous structure, was lower in terms of derivative intensity when compared to the first peak at 280 °C. The enhanced thermal degradation of ODS and the profile alteration of HPβCD in ODS/HPβCD NW were the evidence of drug and CD

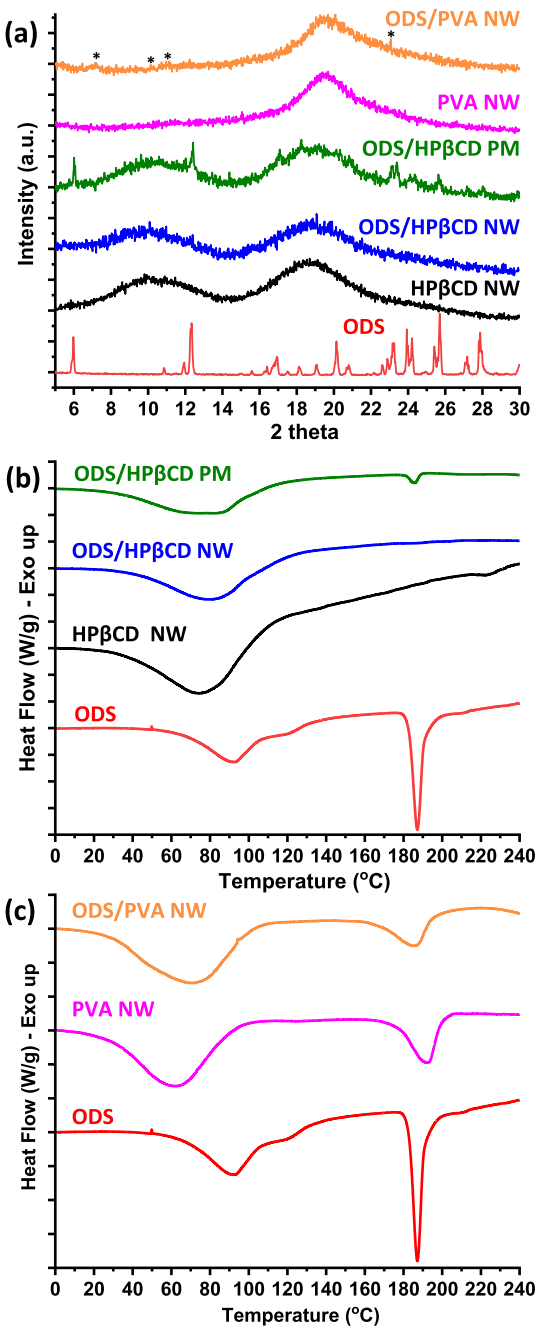

Fig. 4. (a) XRD graphs of ODS, HPβCD NW, ODS/HPβCD NW, ODS/HPβCD PM, PVA NW, and ODS/PVA NW. DSC thermograms of (b) ODS, HPβCD NW, ODS/HPβCD NW, ODS/HPβCD PM, and (c), ODS, PVA NW, and ODS/PVA NW (NW: nanofibrous web; PM: physical mixture).

interaction in a way of encapsulation of ODS in the HPβCD cavity (Mura, 2015). For ODS/HPβCD PM, the first main weight loss step (268 °C) corresponding to the ODS degradation indicated an onset point at 160 °C likewise pure ODS. In addition, the second main weight loss belonging to HPβCD thermal degradation took part at 356 °C by possessing higher derivative intensity compatibly to higher content of HPβCD (~90 %, w/w) in the physical mixture. On the other hand, pristine PVA NW depicted a core weight loss at 320 °C and a small one at 435 °C due to thermal degradation of polymeric matrix (Fig. 5b-i). For ODS/PVA NW, the thermal degradation of ODS started at around 160 °C in the same way as pure ODS powder. However, it was rather obvious that there was a distinct difference in the thermal profile of ODS/PVA NW than the pristine PVA and ODS associated with shifting all peaks to the higher temperature ranges (Fig. 5b-ii). This was also further evidence of interactions between ODS and PVA, as noted earlier in the FTIR (Fig. 3), XRD and DSC (Fig. 4) findings.

3.3. Loading efficiency

The initial molar ratio of ~ 1:2 (drug:CD) was applied to prepare the ODS/HPβCD inclusion complex aqueous system resulting in 8 % (w/w) of ODS in nanofibrous webs. The control sample of ODS/PVA NW was also generated as to include the same amount of ODS (8 % (w/w)). The loading efficiency test was performed by dissolving nanofibrous webs in DMSO. It was found that ODS/HPβCD NW and ODS/PVA NW had loading efficiencies of 95.4 ± 1.3 and 79.9 ± 2.7, respectively. The higher loading efficiency for the ODS/HPβCD NW suggested that more drug molecules was able to be incorporated into the ultimate nanofibrous webs due to inclusion complexation between ODS and HPβCD. The statistical analysis depicted that the means of the two samples are significantly different from each other ($p < 0.05$).

Proton nuclear magnetic resonance (^{1}H NMR) spectroscopy also enabled the calculation of the loading efficiency (%, w/w) of ODS/HPβCD NW roughly and analyze the chemical structure of ODS after the entire process of electrospinning. Fig. 6a indicates the ^{1}H NMR spectra of ODS, HPβCD NW and ODS/HPβCD NW. The integrated area of the highlighted peaks of ODS and HPβCD were used for the calculation, and it was detected that the initial molar ratio of ~ 1:2 (ODS:CD) was preserved and the ODS/HPβCD NW were obtained almost ~ 100 % (w/w) of loading efficiency. This finding was slightly higher than the loading efficiency test result in which this value was determined as ~ 96 (w/w) for ODS/HPβCD NW. In case of ODS/PVA NW, the overlapping of some peaks of ODS and PVA and the alteration observed at the characteristic peaks of ODS disenabled the calculation of approximate loading efficiency using ^{1}H NMR technique. Fig. 6b shows the extended ^{1}H NMR spectra of ODS, ODS/HPβCD NW and ODS/PVA NW at the range of 7.1 and 8.1 ppm. It was obvious that there were significant shifts and pattern differences at the given characteristic peaks of ODS in case of ODS/PVA NW compared to ODS/HPβCD NW (Fig. 6b). The slight shifts of ODS peaks for ODS/HPβCD NW can be assigned to the enveloping of drug molecules into CD cavities by inclusion complexation. Moreover, it was detected that there was a shift at the characteristic peaks of PVA corresponding to proton of hydroxyl groups (Fig. 6c). All these alterations can be attributed to a potential hydrogen bonding between ODS and PVA which was also supported by previous findings of FTIR, XRD, DSC and TGA.

3.4. Computational study

The interaction between ODS and HPβCD was examined by first-principles computational methods. Within this framework, the ions of ODS and HPβCD were first relaxed in vacuum and solvent, and the ground state structures were obtained. Next, the ODS was inserted into HPβCD through the wide (W) and narrow (N) rim. The optimized configurations were obtained at different positions by considering head (H) and tail (T) orientations of ODS (Fig. 7a-c). It should be noted that the total energy (in vacuum and water) decreased as ODS approaches HPβCD, and no energy barrier was recognized. The lowest energy configurations corresponding to ODS/HPβCD- inclusion complex (IC) for 1/1 and 1/2 stoichiometries were presented in Fig. 7d-g. Even ODS/HPβCD-IC can be formed for both orientations of ODS, H orientation through wide rim was energetically more favorable for 1/1 stoichiometry. Similarly, for 1/2 configuration, ODS interacted with the wide rims of both HPβCDs. Following the formation of ODS/HPβCD-IC, the complexation energy can be calculated by using the relation; $E_{CE} = n*E[HP\beta CD] + E[ODS] - E[ODS/HP\beta CD\text{-}IC]$ where E[HPβCD], E[ODS], and E(ODS/HPβCD-IC) are the total energies of HPβCD, ODS, and ODS/HPβCD-IC, respectively. n is the number of HPβCD, which was determined by stoichiometry. The estimated E_{CE}'s listed in Table 2 revealed

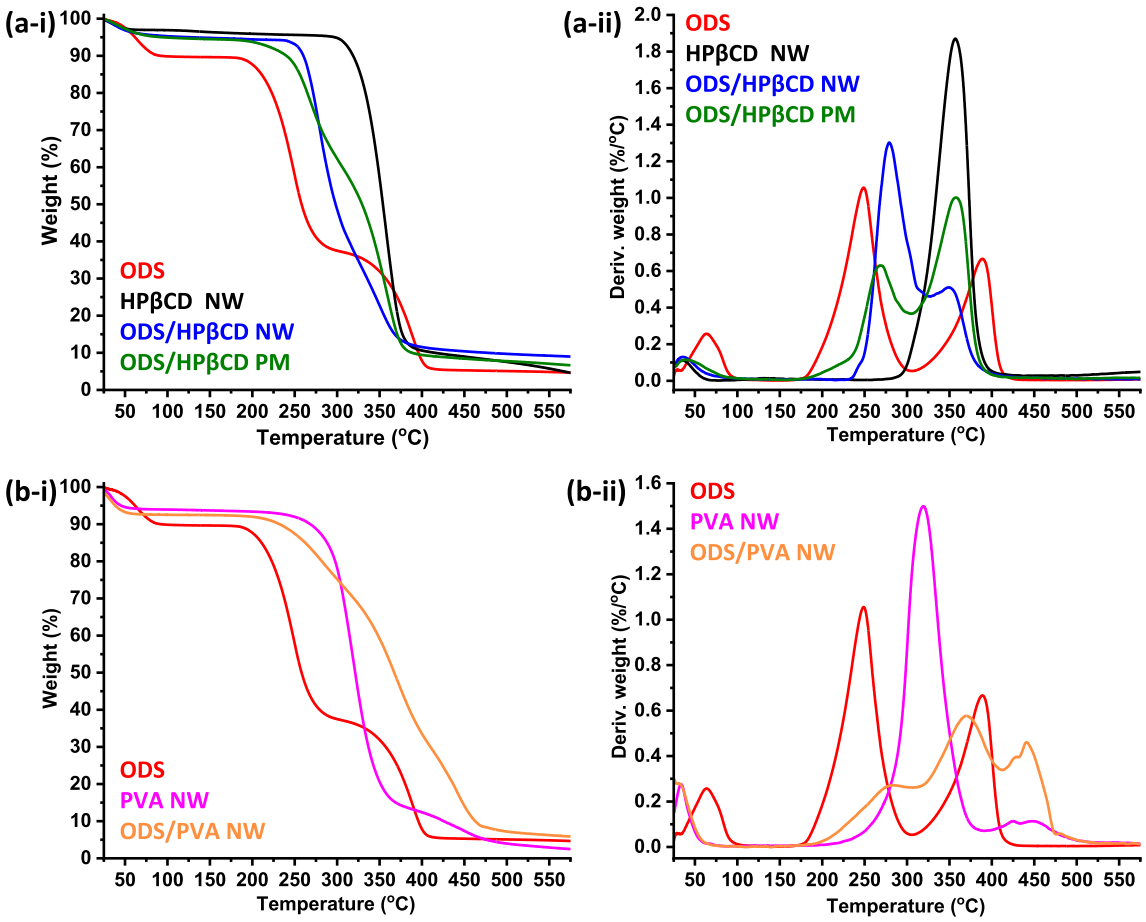

Fig. 5. (i) TGA thermograms and (ii) DTG of (a) ODS, HPβCD NW, ODS/HPβCD NW, ODS/HPβCD PM, and (b), ODS, PVA NW, and ODS/PVA NW (NW: nanofibrous web; PM: physical mixture).

that the stable ODS/HPβCD-IC can be formed both for 1/1 and 1/2 stoichiometries. Even the effect of including water on structures was found to be minor, a significant decrease in E_{CE} with respect to vacuum was observed. The decrease in E_{CE} indicated a reduction in the interaction strength between ODS and HPβCD, which can also be correlated with release rates. On the other hand, it can be concluded that 1/2 stoichiometry was energetically more favorable compared to 1/1 one in both water and vacuum environment. Finally, the solvation energy (E_{SE}) was calculated to reveal the effect of IC formation on the solubility of ODS. E_{SE} can be defined as the difference between the total energy of IC in water and vacuum ($E_{SE} = E^{water}[IC] - E^{vacuum}[IC]$). As listed in Table 2, the E_{SE} of ODS/HPβCD-IC became −88.1 and −155.9 kcal/mol for 1/1 and 1/2 stoichiometries, respectively and this suggested that 1/2 stoichiometry provided better enhancement in solubility than 1/1 stoichiometry.

3.5. Pharmacotechnical profiles of nanofibrous webs

The phase solubility test was performed to analyze the effects of increasing HPβCD concentrations on the solubility of ODS (Fig. 8a). The intrinsic solubility of ODS without HPβCD was denoted as ~ 5.6 mM and ~ 1.7 times higher solubility was achieved with inclusion complexation for the highest HPβCD concentration (160 mM). The binding constants (K_S) between ODS and HPβCD was also calculated as 6.2 M^{-1} by using the phase solubility diagram. In this study, the time-dependent release profiles of ODS/HPβCD NW and ODS/PVA NW were studied in PBS buffer (pH 7.4) and Fig. 8b shows the release graphs of samples. The significantly higher release performance of ODS/HPβCD NW was obvious with ~ 80 % release concentration in 30 s compared to ODS/PVA NW having ~ 0.6 % of ODS release in the same period. Afterwards, the release performance of ODS/HPβCD NW reached to ~ 100 % in 2 min and showed approximately plateau profile over 10 min. On the other hand, ODS/PVA NW only got the release concentration of ~ 24 % at the end of 10 min (Fig. 8b). The noteworthy difference between samples were also confirmed by the statistical analysis ($p < 0.05$). In case of ODS/PVA NW, ODS crystals was encapsulated in a polymeric matrix, and so the release of drug that was also very based on the intrinsic water solubility of ODS molecules (~5.6 mM), occurred by the dissolution of polymeric matrix in the aqueous medium. The crystal state of ODS and the lower water solubility of PVA (~200 mg/mL) polymer compared to HPβCD (>2000 mg/mL) were the main reasons of the lower and slower release of ODS from ODS/PVA NW. As it was revealed by the previous structural characterization, the potential hydrogen bonding formed between PVA and ODS might be also a retarding effect on exuding of drug into the liquid medium from polymeric matrix. These results demonstrated that the inclusion complexation between ODS and HPβCD enabled to attain a better release profile for ODS compared to one encapsulated into a polymeric matrix due to amorphous distribution and so enhanced solubility of ODS. The distinctively higher water solubility of hydroxy-propylated βCD was also one of the main reasons to obtain the higher and faster release of drug molecules by the rapid dissolution of web substrate in the PBS medium. The dissolution behavior of nanofibrous webs was also recorded visually as depicted in Fig. 8c and Video-S1. The significantly faster dissolution of HPβCD based nanofibrous webs compared to PVA ones was also confirmed by this dissolution tests. As seen in captured photos taken in a short time, PVA NW and PVA/ODS NW remained undissolved layer on the top of the water (Fig. 8c-ii) while HPβCD NW and ODS/HPβCD NW

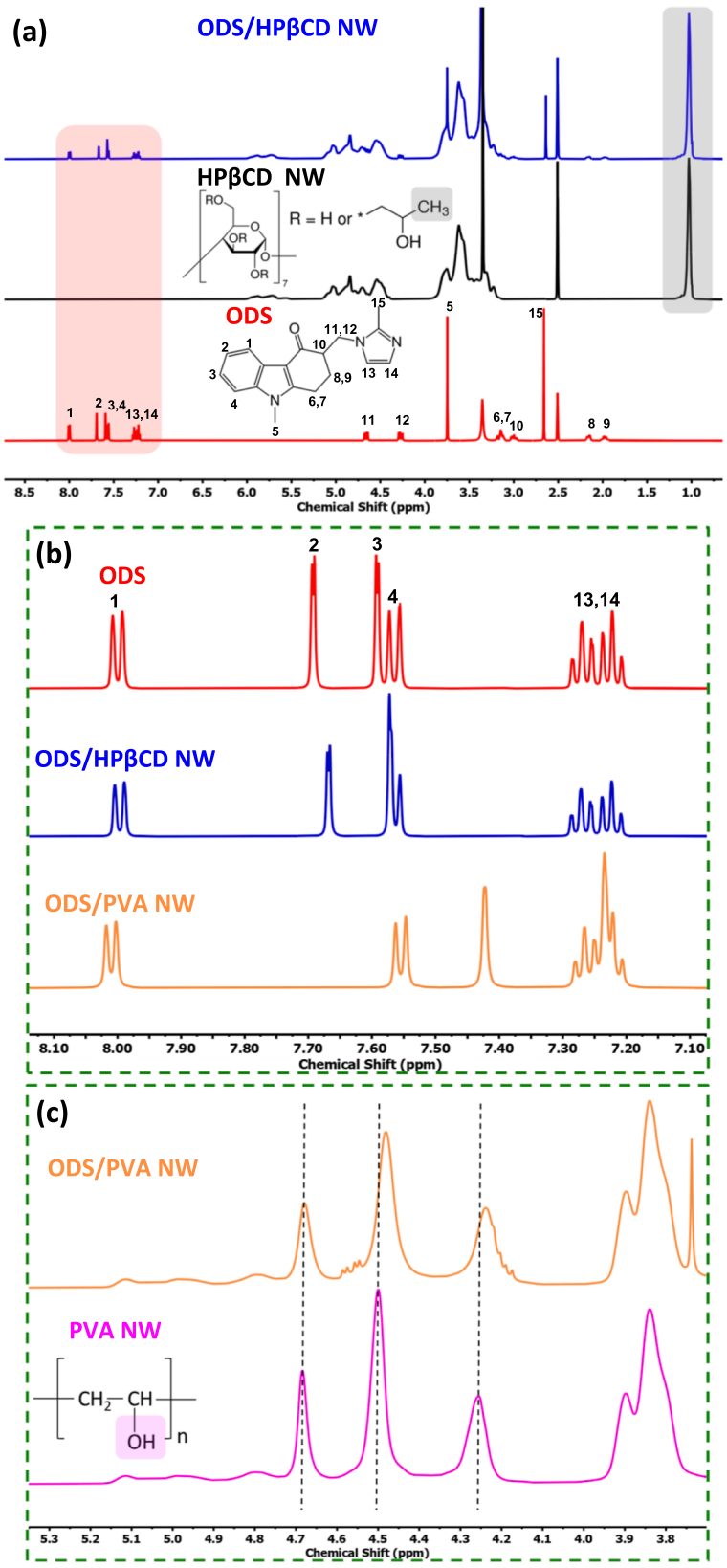

Fig. 6. ^{1}H NMR spectra of (a) ODS, HPβCD NW, ODS/HPβCD NW. Expanded ^{1}H NMR spectra of (b) ODS, HPβCD NW ODS and ODS/PVA NW, and (c) ODS/PVA NW and PVA NW (NW: nanofibrous web).

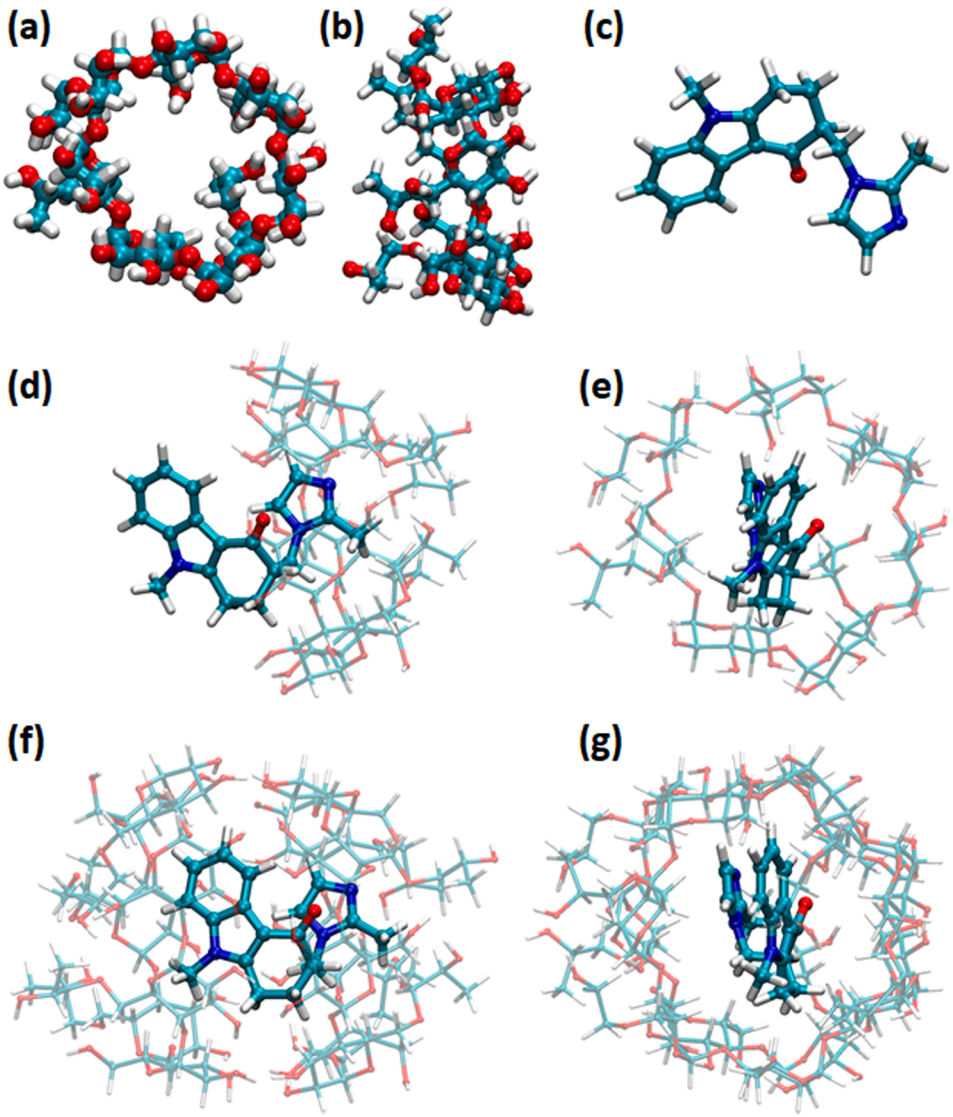

Fig. 7. The top and side views of (a), (b) HPβCD, (c) ODS, (d), (e) ODS/HPβCD-IC for 1/1 and (f), (g) ODS/HPβCD-IC for 1/2 stoichiometry.

Table 2
The complexation and solvation energies of ODS/HPβCD-IC for different orientations in 1/1 and 1/2 stoichiometry. T and H indicate tail and head orientation of ondansetron; N and W indicate narrow and wide rims of HPβCD.

ODS/HPβCD Ratio	Orientation	E_{CE}^{Vacuum} kcal/mol	E_{CE}^{Water} kcal/mol	E_{SE} kcal/mol
1/1	TH-WN	20.59	–	–
	HT-WN	27.03	16.25	−88.06
1/2	NW-TH-NW	60.80	–	–
	NW-TH-WN	88.96	46.30	−136.61

completely dissolved and formed clear solutions in less than a second (Fig. 8c-i).

The release profile of nanofibrous webs was further examined by different kinetic models. The formulations and the result (R^2, regression coefficient) were summarized in supporting information (Table S1). The kinetic model calculations exhibited that the release profile of ODS/HPβCD NW did not fit with the zero/first-order kinetics, Higuchi and Hixson-Crowell models (Table S1). This established that the ODS release did not occur in accordance with Fick's first law showing a time-dependent release from an insoluble planar matrix (Peppas and Narasimhan, 2014). On the other hand, comparatively higher consistency was observed with Korsmeyer–Peppas model supporting the erosion and diffusion-controlled release of ODS from ODS/HPβCD NW. The diffusion exponent (n) value calculated using the Korsmeyer–Peppas equations was detected in the range of $0.45 < n < 0.89$ for ODS/HPβCD NW and this also pointed the non-Fickian or irregular diffusion of ODS from nanofibrous webs (Peppas and Narasimhan, 2014). For ODS/PVA NW, the release profile depicted coherence with almost all kinetic models taking part in calculations except Korsmeyer–Peppas (Table S1). This promoted that the release of ODS was dominated by the Fickian diffusion mechanism and the progressive disintegration of matrix as a function of time (Gouda et al., 2017; Peppas and Narasimhan, 2014).

The disintegration performance of the nanofibrous webs was evaluated in simulated environment of oral cavity created with filter paper wetted with artificial saliva (Balusamy et al., 2020). Fig. 9 depicted the photos captured from Video-S2 and Video-S3. HPβCD NW and ODS/HPβCD NW were absorbed within two seconds upon contact with the filter papers (Fig. 9a, b). In comparison, the PVA and ODS/PVA NW did not rapidly disintegrate, even after 50 s thin layer of nanofibrous webs remained on the filter papers (Fig. 9c, d). Essentially, the high porosity and high surface area of nanofibrous webs forms active interaction sides for liquid medium and this contributes to the penetration of medium through the fiber structures during dissolution and disintegration (Yu et al., 2018). In case of ODS/PVA NW, the lower solubility of PVA matrix

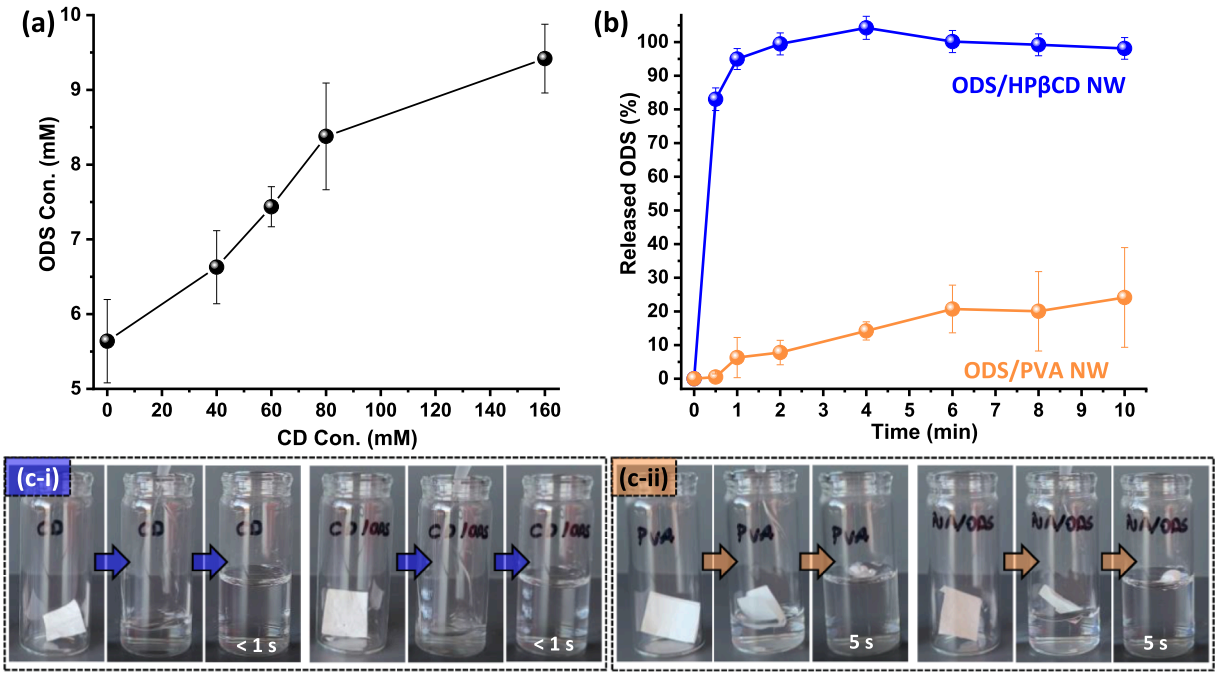

Fig. 8. (a) Phase solubility diagram of ODS against increasing HPβCD concentrations. (b) Time-dependent release profile of ODS/HPβCD NW and ODS/PVA NW. (c) The dissolution profiles of (captured from Video-S1) (i) HPβCD NW and ODS/HPβCD NW, and (ii) PVA NW ODS/PVA NW (NW: nanofibrous web).

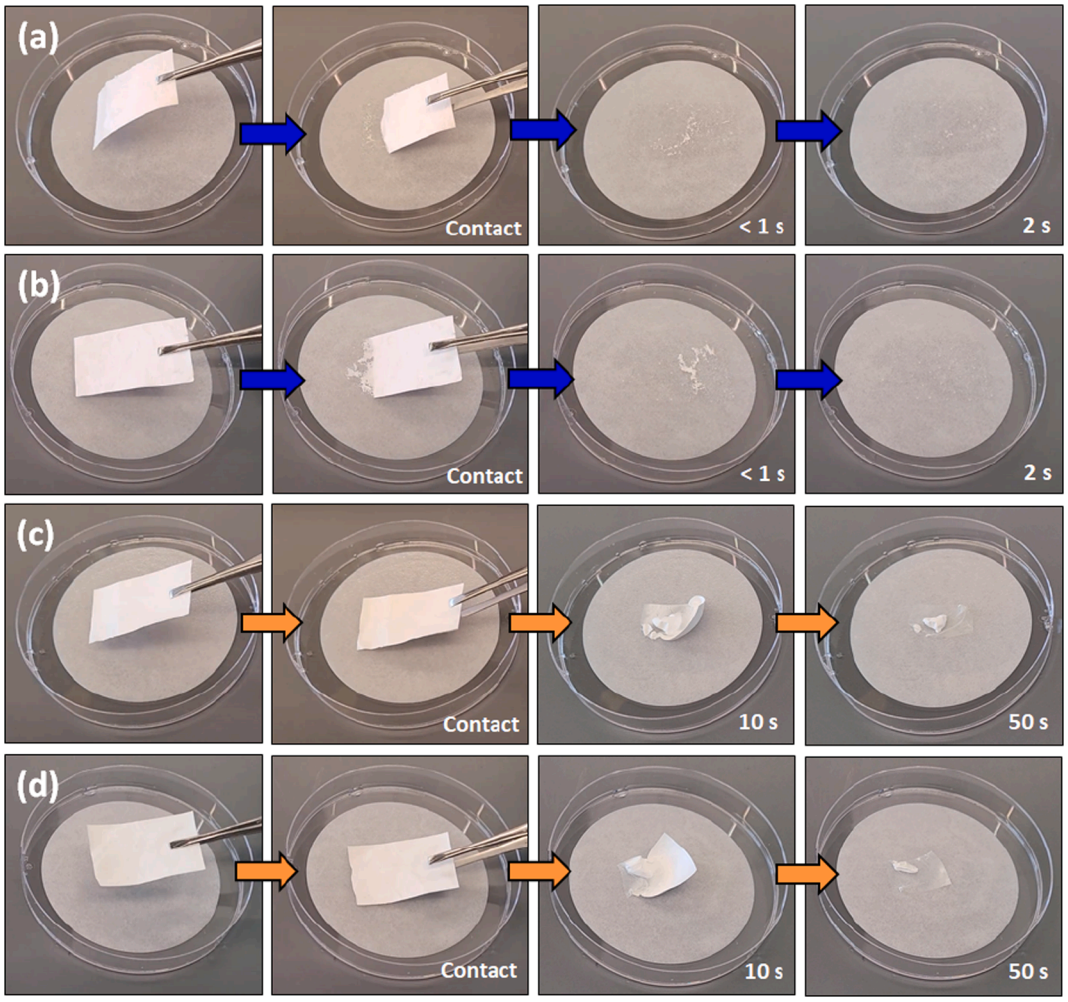

Fig. 9. Disintegration profiles of (a) HPβCD NW, (b) ODS/HPβCD NW, (c) PVA NW, and (d) ODS/PVA NW (captured from Video-S2 and S3) (NW: nanofibrous web).

and the crystalline content of ODS in the nanofibrous web also latened the disintegration of samples when compared with HPβCD based samples. In other words, the highly water-soluble nature of HPβCD raised an advantageous dynamic for the fast disintegration of nanofibrous webs, as well (Loftsson and Brewster, 2010). Thus, ODS/HPβCD NW would be more suitable as an oral fast-disintegrating delivery system for ODS than a PVA-based one, as it would disintegrate rapidly and entirely without resulting a granular feeling in the oral cavity during administration.

4. Conclusions

In this study, ODS/HPβCD NW enabled the amorphous distribution of ODS in the fibrous matrix by the non-covalent interaction of inclusion complexation with CD cavity. On the other hand, ODS crystals were embedded into polymeric PVA NW along with an additional hydrogen bonding between ODS and PVA chains. The initial drug loading was ~ 8 % (w/w) for both nanofibrous webs, however, ODS/HPβCD NW was obtained with higher loading efficiency (~96 %, w/w) compared to ODS/PVA NW (~80 %, w/w) due to inclusion complexation. The superior features of nanofibers such as high porosity and high surface area, the amorphous state of ODS by inclusion complexation, and significantly high solubility of HPβCD (>2000 mg/mL) provided faster dissolution/disintegration of electrospun web in aqueous medium/artificial saliva and better release of ODS from ODS/HPβCD NW compared to ODS/PVA NW. ODS/HPβCD NW was produced without using an additional toxic solvent or compounds in water and this can be considered as great prospect for the industrialization of this new dosage formulations. Briefly, inclusion complex nanofibrous web can be implemented for the antiemetic drug molecule of ODS effectively. The orally fast-disintegrating ODS/HPβCD NW might be a promising alternative to the commercial dosage formulations of orally fast-disintegration ODS tablets. Even, the unfavorable taste of ODS which can disturb the compliance of the patient can be also removed by inclusion complexation. To conclude, ODS/HPβCD NW might be attractive during the treatment of nausea and vomiting to be free of chewing and swallowing complications and without a granular feeling in the oral cavity.

CRediT authorship contribution statement

Emmy Hsiung: Investigation, Writing – original draft. **Asli Celebioglu:** Conseptualization, Methodology, Investigation, Writing – original draft. **Mehmet Emin Kilic:** Investigation and writing of computational modeling study. **Engin Durgun:** Investigation and writing of computational modeling study. **Tamer Uyar:** Conseptualization, Methodology, Editing final version, Funding acquisition, Project administration.

Declaration of Competing Interest

The authors declare that they have no known competing financial interests or personal relationships that could have appeared to influence the work reported in this paper.

Data availability

Data will be made available on request.

Acknowledgement

This work made use of the Cornell Center for Materials Research Shared Facilities which are supported through the NSF MRSEC program (DMR-1719875), and the Cornell Chemistry NMR Facility supported in part by the NSF MRI program (CHE-1531632), and Department of Human Centered Design facilities. M.E.K acknowledges support from Brain Pool Program through the National Research Foundation of Korea (NRF) funded by the Ministry of Science and ICT (2020H1D3A1A02081517).

Appendix A. Supplementary data

Supplementary data to this article can be found online at https://doi.org/10.1016/j.ijpharm.2022.121921.

References

Adepu, S., Ramakrishna, S., 2021. Controlled drug delivery systems: current status and future directions. Molecules 26 (19), 5905. https://doi.org/10.3390/molecules26195905.

Akhgari, A., GHALAMBOR, D.A., Rezaei, M., Kiarsi, M., ABBASPOUR, M.R., 2016. The design and evaluation of a fast-dissolving drug delivery system for loratadine using the electrospinning method.

Baghel, P., Roy, A., Chandrakar, S., Bahadur, S., 2013. Fast dissolving drug delivery systems: a brief review. Res. J. Pharm. Technol. 6, 597–602.

Balusamy, B., Celebioglu, A., Senthamizhan, A., Uyar, T., 2020. Progress in the design and development of "fast-dissolving" electrospun nanofibers based drug delivery systems - A systematic review. J. Control. Release 326, 482–509.

Blöchl, P.E., 1994. Projector augmented-wave method. Phys. Rev. B 50 (24), 17953–17979.

Celebioglu, A., Uyar, T., 2021. Electrospun formulation of acyclovir/cyclodextrin nanofibers for fast-dissolving antiviral drug delivery. Mater. Sci. Eng. C 118, 111514. https://doi.org/10.1016/j.msec.2020.111514.

Celebioglu, A., Uyar, T., 2020. Hydrocortisone/cyclodextrin complex electrospun nanofibers for a fast-dissolving oral drug delivery system. RSC Med. Chem. 11 (2), 245–258.

Celebioglu, A., Uyar, T., 2019a. Metronidazole/Hydroxypropyl-β-Cyclodextrin Inclusion Complex Nanofibrous Webs as Fast-dissolving Oral Drug Delivery System. Int. J. Pharm. 572, 118828. https://doi.org/10.1016/j.ijpharm.2019.118828.

Celebioglu, A., Uyar, T., 2019b. Fast Dissolving Oral Drug Delivery System based on Electrospun Nanofibrous Webs of Cyclodextrin/Ibuprofen Inclusion Complex Nanofibers. Mol. Pharm. 16 (10), 4387–4398.

Celebioglu, A., Wang, N., Kilic, M.E., Durgun, E., Uyar, T., 2021. Orally Fast Disintegrating Cyclodextrin/Prednisolone Inclusion-Complex Nanofibrous Webs for Potential Steroid Medications. Mol. Pharm. 18 (12), 4486–4500. https://doi.org/10.1021/acs.molpharmaceut.1c0067710.1021/acs.molpharmaceut.1c00677.s00110.1021/acs.molpharmaceut.1c00677.s00210.1021/acs.molpharmaceut.1c00677.s00310.1021/acs.molpharmaceut.1c00677.s004.

Cho, E., Gwak, H., Chun, I., 2008. Formulation and evaluation of ondansetron nasal delivery systems. Int. J. Pharm. 349 (1-2), 101–107.

Crini, G., 2014. A history of cyclodextrins. Chem. Rev. 114, 10940–10975. https://doi.org/10.1021/cr500081p.

Gouda, R., Baishya, H., Qing, Z., 2017. Application of mathematical models in drug release kinetics of carbidopa and levodopa ER tablets. J. Dev. Drugs 6, 1–8. https://doi.org/10.4172/2329-6631.1000171.

Gould, S., Scott, R.C., 2005. 2-Hydroxypropyl-β-cyclodextrin (HP-β-CD): a toxicology review. Food Chem. Toxicol. 43 (10), 1451–1459.

Grimme, S., 2006. Semiempirical GGA-type density functional constructed with a long-range dispersion correction. J. Comput. Chem. 27 (15), 1787–1799.

Hohenberg, P., Kohn, W., 1964. Inhomogeneous electron gas. Phys. Rev. 136 (3B), B864–B871.

Illangakoon, U.E., Gill, H., Shearman, G.C., Parhizkar, M., Mahalingam, S., Chatterton, N.P., Williams, G.R., 2014. Fast dissolving paracetamol/caffeine nanofibers prepared by electrospinning. Int. J. Pharm. 477 (1-2), 369–379.

Itoh, H., Li, Y.i., Chan, K.H.K., Kotaki, M., 2016. Morphology and mechanical properties of PVA nanofibers spun by free surface electrospinning. Polym. Bull. 73 (10), 2761–2777.

Kamranpour, S., Mirzaeei, S., Daneshgar, F., Najafi, F., 2021. Fast-dissolving Sublingual Nanofibers of Ondansetron Hydrochloride: Formulation, Physicochemical Characterization, and Clinical Evaluation on Post-cataract Surgery Patients. Pharm Sci. https://doi.org/10.34172/PS.2021.24.

Kanouni, K.E., Benguerba, Y., Erto, A., 2019. Theoretical investigation of the solubility of some antiemetic drugs. J. Mol. Liq. 282, 626–632.

Kohn, W., Sham, L.J., 1965. Self-consistent equations including exchange and correlation effects. Phys. Rev. 140 (4A), A1133–A1138.

Kresse, G., Furthmüller, J., 1996. Efficient iterative schemes for ab initio total-energy calculations using a plane-wave basis set. Phys. Rev. B 54 (16), 11169–11186.

Loftsson, T., Brewster, M.E., 2010. Pharmaceutical applications of cyclodextrins: basic science and product development. J. Pharm. Pharmacol. 62, 1607–1621.

Manuel, C.B.J., Jesús, V.G.L., Aracely, S.M., 2016. Electrospinning for drug delivery systems: Drug incorporation techniques. Electrospinning-Material, Tech, Biomed. Appl, p. 14.

Mathew, K., Singh, A.K., Gabriel, J.J., Choudhary, K., Sinnott, S.B., Davydov, A.V., Tavazza, F., Hennig, R.G., 2016. MPInterfaces: A Materials Project based Python tool for high-throughput computational screening of interfacial systems. Comput. Mater. Sci. 122, 183–190.

Mathew, K., Sundararaman, R., Letchworth-Weaver, K., Arias, T.A., Hennig, R.G., 2014. Implicit solvation model for density-functional study of nanocrystal surfaces and reaction pathways. J. Chem. Phys. 140 (8), 084106. https://doi.org/10.1063/1.4865107.

Mura, P., 2015. Analytical techniques for characterization of cyclodextrin complexes in the solid state: A review. J. Pharm. Biomed. Anal. 113, 226–238.
Peppas, N.A., Narasimhan, B., 2014. Mathematical models in drug delivery: How modeling has shaped the way we design new drug delivery systems. J. Control. Release 190, 75–81. https://doi.org/10.1016/j.jconrel.2014.06.041.
Perdew, J.P., Burke, K., Ernzerhof, M., 1997. Generalized gradient approximation made simple. Phys. Rev. Lett 78, 1396.
Preis, M., 2015. Orally disintegrating films and mini-tablets—innovative dosage forms of choice for pediatric use. Aaps Pharmscitech 16 (2), 234–241.
Saokham, P., Muankaew, C., Jansook, P., Loftsson, T., 2018. Solubility of cyclodextrins and drug/cyclodextrin complexes. Molecules 23 (5), 1161. https://doi.org/10.3390/molecules23051161.
Seif, S., Franzen, L., Windbergs, M., 2015. Overcoming drug crystallization in electrospun fibers–Elucidating key parameters and developing strategies for drug delivery. Int. J. Pharm. 478 (1), 390–397.
Singh, A., Ansari, V.A., Haider, F., Ahsan, F., Mahmood, T., Maheshwari, S., Tiwari, R.K., 2021. Oral fast dissolving film: The avant-garde avenue for oral consignment modus operandi. Res. J. Pharm. Technol. 14, 2145–2152.
Sung, Y.K., Kim, S.W., 2020. Recent advances in polymeric drug delivery systems. Biomater. Res. 24, 1–12.
Tanveer, S., Ahmad, M., Minhas, M.U., Ahmad, A., Khan, K.U., 2021. Chitosan-PVA-co-poly (2-Acrylamido-2-Methylpropane Sulfonic Acid) Cross-linked Hybrid IPN-Nanogels for Transdermal Delivery of Ondansetron; Synthesis, Characterization and Toxicological Evaluation. Polym. Technol. Mater. 60, 1913–1934.
Teaima, M.H., El Mohamady, A.M., El-Nabarawi, M.A., Mohamed, A.I., 2020. Formulation and evaluation of niosomal vesicles containing ondansetron HCL for trans-mucosal nasal drug delivery. Drug Dev. Ind. Pharm. 46 (5), 751–761.
Vuddanda, P.R., Mathew, A.P., Velaga, S., 2016. Electrospun nanofiber mats for ultrafast release of ondansetron. React. Funct. Polym. 99, 65–72.
Wang, Y., Deng, Z., Wang, X., Shi, Y., Lu, Y., Fang, S., Liang, X., 2021. Formononetin/methyl-β-cyclodextrin inclusion complex incorporated into electrospun polyvinyl-alcohol nanofibers: Enhanced water solubility and oral fast-dissolving property. Int. J. Pharm. 603, 120696. https://doi.org/10.1016/j.ijpharm.2021.120696.
Xue, J., Wu, T., Dai, Y., Xia, Y., 2019. Electrospinning and electrospun nanofibers: Methods, materials, and applications. Chem. Rev. 119 (8), 5298–5415. https://doi.org/10.1021/acs.chemrev.8b00593.
Yu, D.-G., Branford-White, C., Shen, X.-X., Zhang, X.-F., Zhu, L.-M., 2010a. Solid dispersions of ketoprofen in drug-loaded electrospun nanofibers. J. Dispers. Sci. Technol. 31 (7), 902–908.
Yu, D.-G., Li, J.-J., Williams, G.R., Zhao, M., 2018. Electrospun amorphous solid dispersions of poorly water-soluble drugs: A review. J. Control. Release 292, 91–110.
Yu, D.-G., Yang, J.-M., Branford-White, C., Lu, P., Zhang, L.i., Zhu, L.-M., 2010b. Third generation solid dispersions of ferulic acid in electrospun composite nanofibers. Int. J. Pharm. 400 (1-2), 158–164.
Yu, D.-G., Zhang, X.-F., Shen, X.-X., Brandford-White, C., Zhu, L.-M., 2009. Ultrafine ibuprofen-loaded polyvinylpyrrolidone fiber mats using electrospinning. Polym. Int. 58 (9), 1010–1013.
Yuan, C., Liu, B., Liu, H., 2015. Characterization of hydroxypropyl-β-cyclodextrins with different substitution patterns via FTIR, GC–MS, and TG–DTA. Carbohydr. Polym. 118, 36–40.
Zhu, Y., Zhang, Q., Zou, J., Wan, M., Zhao, Z., Zhu, J., 2015. Pharmacokinetics and bioavailability study of two ondansetron oral soluble film formulations in fasting healthy male Chinese volunteers. Drug Des. Devel. Ther. 9, 4621.